Modifying Irregular Titania Powders in a Low Power Microwave Plasma Torch

Ganesh Vanamu, Kelvin Lester, and Abhaya K. Datye
University of New Mexico, Dept. of Chemical and Nuclear Engineering Farris Engineering Center, Albuquerque, NM 87131

John C. Weigle, Chun-Ku Chen, Daniel Kelly, and Jonathan Phillips
Los Alamos National Laboratory, Los Alamos, NM 87545

DOI 10.1002/aic.10244
Published online in Wiley InterScience (www.interscience.wiley.com).

Rapid passage of titania powder as an aerosol through a plasma generated with a low power microwave torch, resulted in many changes to the powder. Some or all of the titania became spherical, its phase changed, the level of carbon impurity changed, and its surface area declined. The final state of the titania depended on plasma operating conditions. For example, all of the titania became spherical and converted to the rutile phase, only if the processing rate remained low. Complete spherodization occurred only if the energy absorbed by the particles was <2.5% of the total power applied. Excess solid loading reduced the fraction spherodized or otherwise modified, as well as the net rate of conversion. Passing titania through an oxygen plasma removed virtually all the carbon impurity. This process is similar to alumina studies in the same apparatus and suggests that many refractory oxides can be modified by low-power plasmas. © 2004 American Institute of Chemical Engineers *AIChE J,* 50: 2090–2100, 2004
Keywords: titania, plasma processing, phase transformation, purification, photocatalysis

Introduction

The use of high-power (>25 kW) plasmas to process ceramics is an established technology, particularly for the production of films and coatings. There are numerous studies of sintering alumina and other oxides in high-power plasmas (Cordone and Martinsin, 1972; Thomas and Freim, 1975; Johnson and Rizzo, 1980; Ishigaki et al., 1993; Gell et al., 2001; Bennett et al; 1968). In addition, recent studies showed that ceramics could be made directly from precursor molecular species using high-power plasmas (Ananthapadmanabhan et al., 1999; Fauchais et al., 1997). However, our group is the first to focus on the use of a low-power (<1 kW) plasma with an aerosol feed to generate unique ceramic particles. In an earlier study, we demonstrated that a plasma torch could be employed to generate spherical alumina particles of controlled size using irregularly shaped alumina particles, passed through the torch in an aerosol, as precursors (Chen 1999; Chen 2001; Phillips 1999). Data were collected regarding the impact of residence time in the plasma, power levels, and solid fraction on the phase of alumina, and the degree of spherodization. Particle size increased with the solid fraction of the input aerosol, and the amount of power absorbed. As the solid mass flow rate was increased above a measured maximum, the fraction of alumina spherodized decreased. The phases found in the product were a strong function of the operating conditions.

In this work, we have quantitatively examined the impact of plasma torch operating conditions on the spherodization, phase, surface area, and ultimate purity of titania. In this case, the input material was a highly irregularly shaped, high surface area material. Titania was chosen as a second example of refractory oxide modification, because of the widespread applications of the material as a component of paint (Carter et al., 1998; Diebold, 1995; Wicks et al., 2001; Gaumet et al; 1997; Sadasivan and Ghandi, 2001), and as a photocatalyst (Fox and Dulay, 1993; Martin et al.,1995; Premkumar and Ramaraj,

Correspondence concerning this article should be addressed to J. Phillips at phillips@lanl.gov.

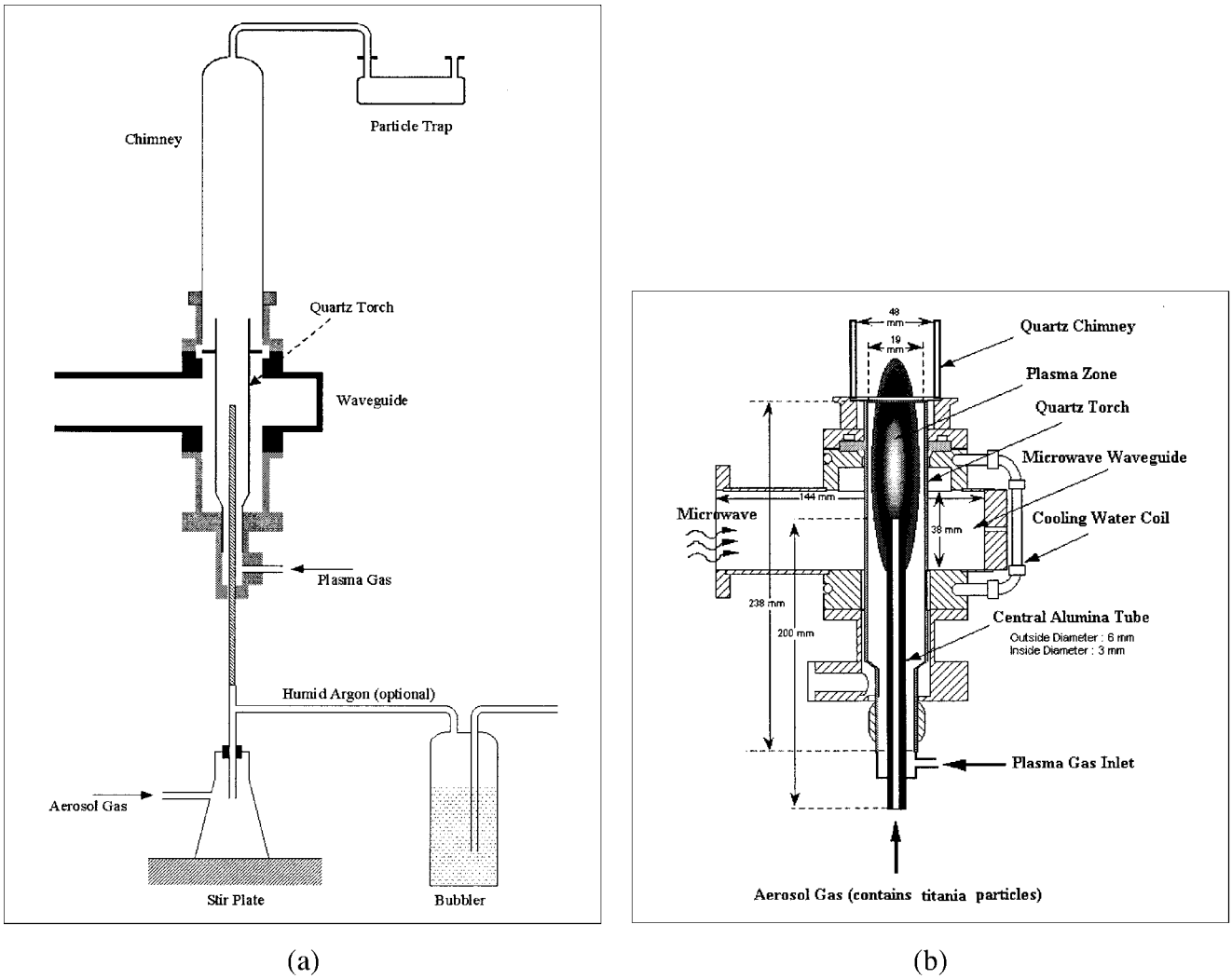

Figure 1. Low power microwave plasma torch.

(a) Equipment configuration, including the stirred particle feeder (dry feed entering the torch), and (b) coupler region of the microwave plasma torch system (Chen, 1999).

1997; Ameta et al., 1994; Rao and Dube, 1996; Ziolli and Jardim, 1998). Indeed, preliminary studies indicate that the plasma-treated titania is significantly more active for some photocatalytic reactions than the precursor (P-25). The characterization work presented here suggests the enhanced activity may arise from phase change, surface area reduction, or segregation of impurities. Attributing the increased activity to any one factor or combination of factors is premature. Finally, using a precursor powder made up of nanoscale particles tested the hypothesis that very small particles do not agglomerate in plasmas due to particle charging and the subsequent electrostatic repulsion.

The process of spherodization of titania was found to be qualitatively similar to that of alumina. Evidence indicates that, for both materials, spherodization occurs via the sequence of melting, agglomeration, and refreezing. In both cases, spherodization correlated with surface area reduction. There was some evidence that particle charging affected the agglomeration process, but a simple model reveals that a more detailed characterization of the plasma, and of the particle dynamics are necessary to understand charging effects fully. Moreover, the phase of the spherodized product is different from that of the input phase. There were also quantitative similarities, such as the finding that only a few percent of the absorbed plasma energy was used for the spherodization process. One novel finding was that, for the titania employed, the plasma treatment drew impurities, particularly carbon, to the particle surface. Also, for the first time, it was demonstrated that individual spherodized particles can contain multiple phases. Overall, the results confirm that the plasma torch can be used as a tool for the modification of a host of oxide ceramics.

Experimental

A low power microwave plasma torch (MKS/Astex, 1 kW, 19 mm ID) was used to generate oxygen and argon plasmas at atmospheric pressure. The equipment is depicted in Figure 1; all details of the system are described elsewhere (Shim et al., 1999). Using a three-stub tuner, power is coupled into the gas (directly to the electrons, and then to the neutral species and

ions) as it passes through the waveguide, hence, creating an atmospheric pressure plasma. The key feature of the system is the availability of two atmospheric pressure gas flows. The aerosol containing flow (aerosol gas) passes coaxially through a 3 mm ID alumina tube that ends near the center of the microwave waveguide. The second gas (plasma gas) is the outer flow, contained within a 19 mm OD quartz torch. The two flows join at the center of the microwave (2.45GHz) waveguide, very near the hottest point in the plasma, $T_{rot}>3000$ K (Chen 1999). It is estimated that the aerosol particles spend less than 0.1 s in the high-temperature zone of the plasma, before emerging from the torch and flowing into a 4 cm dia. by 25 cm height Pyrex chimney attached to the plasma waveguide with an O-ring compression clamp.

Precursor titania was fed through the plasma torch as an aerosol. The titania was Degussa P-25, a standard photocatalyst composed of primary particles with an average size of 25 nm. The aerosols were generated using a simple stirred particle feeder (Figure 1a). A cloud of titania is created in the feeder flask by the combined action of the magnetic stirring bar and the aerosol gas flow. The concentration of solid, always $<1\%$ by volume, was controlled with changes in the power input to the microwave, aerosol gas flow rate, and stirrer speed. All three were empirically found to impact the solid flow rate. The solid is converted as it passes through the torch, and is collected in a particle trap downstream from the chimney.

To test the impact of operating conditions on the character of the product particles, the following parameters were varied: power input to the plasma, aerosol gas flow rate, identity of the plasma gas, stirrer speed, and humidity of the aerosol gas. Plasma gas flow was kept constant in all cases. Each experiment was run for 15 to 60 min, depending on the solid flow rate. The mass of the particles collected in the trap was measured using a balance. The mass flow was obtained by dividing the mass collected by the run time.

The following techniques were employed to determine characteristics of the plasma treated titania: scanning electron microscopy (SEM) using a HITACHI S-800, transmission electron microscopy and selected area diffraction (TEM-SAD) using a JEOL 2010, chemical analysis via XPS, and the dry combustion method (Nelson). Surface analysis was obtained via XPS, using an ultra-high vacuum chamber, with a base pressure of approximately 2×10^{-10} Torr. Bulk chemical analysis was conducted via the dry combustion method. The qualitative trends measured were the same for both techniques, but the absolute values were not. The XPS data were obtained using a nonmonochromatic Mg Kα source. Depth profiling was performed using a differentially pumped Xe^+ ion beam. Powder samples were analyzed by X-ray diffraction (XRD) using a Scintag Pad V diffractometer. BET surface area (Brunauer) was measured using a 2360 Micromeritics Gemini surface analyzer.

The SEM images were used to determine the fraction of titania spherodized, the particle size distribution (PSD) of the spheres, and the energy efficiency of the process. Particle-size distributions and the fraction of material spherodized were obtained using NIH Image software, which calculates the area of individual particles in a micrograph. Approximately 350 particles were analyzed for the PSDs. The fraction spherodized was calculated as the area of spherical particles divided by the total particle area in the micrograph. Once the fraction of material spherodized was determined, the percent energy efficiency was determined using the following formula:

$E \equiv (C_p(T_2 - T_1) + L) * m * S/P$

C_p = specific heat capacity of titania (0.7 J/g.K)
T_2 = melting temperature of titania (1830°C)
T_1 = room-temperature (20°C)
L = latent heat of fusion of titania (3500 J/g)
m = mass flow rate of titania (g/s)
S = fraction of titania spherodized
P = absorbed power

Using the reference intensity ratio (RIR) method, also called internal standard method (Cullity), XRD analysis provided quantitative information regarding the fraction of each phase present in the product. In this method, the strongest line on the XRD pattern of the sample is compared with the strongest line from a single standard reference material. The reference material chosen was α-Al_2O_3 (corundum). I/I_{cor} was determined from a mixture of equal parts by weight of the compound and corundum. The value of I/I_{cor} for any particular compound establishes a single point on the calibration curve of that compound. I is the maximum intensity of the strongest line from the compound, and I_{cor} is the intensity of the corundum. The areas of the peaks from the titania powders could be used with the I/I_{cor} factors to estimate the weight fraction of each phase using the methods described in standard XRD texts (Cullity, 1978).

The RIR method does not provide information regarding the phase composition of individual particles, only the average for the entire sample. To obtain individual particle analysis, thin sections of plasma-generated spheres were prepared according to a protocol described elsewhere (Williams and Carter, 1996). Once the thin sections were prepared, analysis of the phase composition of small areas within single particles was straightforward via TEM-SAD.

Results

Below we discuss five aspects of titania transformation as a function of operating parameters: particle shape, surface area, phase change, energy efficiency of spherodization, and impurity concentration. Variation in aerosol gas flow rate, aerosol particle density, plasma gas identity (argon or oxygen), and applied power all impacted the output particles. Table 1 summarizes the results.

As shown in Figure 2, the plasma treatment dramatically transforms the particle shape and structure. It can be seen that after plasma treatment, the titania is largely spherical, and that the spherical particles have little apparent texture. It is also notable that the nonspherodized material appears to form micron-scale agglomerates; there was no evidence of isolated primary particles. Also, a given titania particle was either completely spherical or else its shape was unaffected. In other words, no partially spherodized particles were observed. Figure 3 reveals that the percentage of the titania spherodized decreases as the aerosol gas flow rate increases. Additionally, higher power leads to a higher percentage of spherodized material at a given flow rate. In appearance, the spherodized titania is identical in all cases. Yet surface area measurements, XRD, and TEM-SAD all indicate that, despite the superficial similarity of spherical appearance, the underlying structures of the particles are quite different and very dependent on the operating parameters employed to produce them.

Measurements of surface area changes (Figure 4) are qual-

Table 1. Summary of Experimental Conditions and Results

Sample No.	Power (W)	Aerosol Gas Flow (slpm)	Solid Flow (g/h)	% Spheres	Avg. Dia. (μm)
1	600	1.73	1.10	~0	4
2	600	1.17	0.64	51	6
3	600	1.54	0.90	17	6
4	600	1.73	0.95	7	4
5	600	0.99	0.56	60	7
6	600	1.17	0.64	52	9
7	600	0.45	0.33	99	10
8	600	0.81	0.42	80	9
9	600	1.54	0.52	66	6
10	600	1.36	0.79	24	7
11	700	1.73	0.90	22	5
12	700	1.17	0.50	76	8
13	700	1.73	0.88	36	6
14	700	1.54	0.80	45	7
15	700	1.73	0.91	6	4
16	700	1.36	0.68	48	8
17	700	0.45	0.37	97	10
18	700	0.45	0.34	98	11
19	700	0.63	0.39	94	10
20	700	0.63	0.42	92	9
21	700	0.99	0.47	82	8

Constant plasma gas flow rate of 1.54 slpm.

itatively consistent with the earlier studies of alumina surface area as a function of treatment (Shim et al., 1999). That is, at higher powers or longer residence times (slower flow rates), the surface area is more severely reduced. Interestingly, when titania is processed through an oxygen plasma, the surface area is greater than when it is processed through an analogous argon plasma.

XRD results clearly show that the phase of the material produced is strongly impacted by operating conditions (Figures 5 and 6). The input material is primarily anatase with some rutile (Ohno et al., 2001), and our quantitative analysis is in agreement with the specifications provided by the manufacturer (80% anatase, 20% rutile). Following passage through the torch at relatively long residence times and high applied power, the material is converted entirely to highly crystalline rutile phase. Treatment at intermediate conditions produced mixtures of anatase and rutile crystals.

The fact that XRD results are averaged over the entire sample leads to another question: Are individual spheres always of a single phase, or can several phases co-exist in a single particle? The answer to this question may have a bearing on the photocatalytic behavior of the titania. Several groups have suggested that particles consisting of multiple phases may exhibit unusual catalytic properties (Bacsa and Kiwi, 1998; Hurum et al., 2001). Thus, to determine the phase composition of individual particles, we employed TEM-SAD.

Detailed studies of more than 20 particles using SAD clearly show that many of the spherical particles contain more than one phase, as shown in Figure 7. That is, particles from some of the highly crystalline samples clearly contain both anatase and rutile material (Figure 7b). In the diffraction pattern, seen in Figure 7b, there are a series of double planes of both anatase and rutile. This is a very clear indication that both phases are present within a single particle.

As shown in Figure 8, the energy efficiency of converting titania to spheres varies from 0.1 to 2.7%. This result is consistent with the energy efficiency for converting alumina to spheres, shown in the earlier work to be between 0.5 and 3% (Chen, 1999; Chen, 2001; Shim et al., 1999).

The efficiency of the process for spherodization was found to be a function of the mass flow rate, the aerosol gas flow rate, and absorbed power. For example, for all three flow rates (Figure 8) there was an optimum mass flow rate. Above or below this rate the measured efficiency was lower. The efficiency is also optimum at a gas flow rate of approximately 0.5 slpm. Efficiency also relates to the percentage spheres that are formed (Figure 9). There is clearly a maximum mass of titania that can be spherodized at a given set of plasma operating conditions. Once the maximum allowed load for any set of operating conditions is surpassed, the percentage spherodized decreases.

Another similarity in spherodization behavior between titania and alumina is the impact of operating conditions on the sphere size (Figure 10). As shown in Table 1 and Figure 10, the average sphere size for titania decreased as the gas flow rate increased. It increased slightly as the power input to the microwave increased from 600 to 700 W. Examples of the particle-size distributions are shown in Figure 11. The particle-size distributions are not well fit by log-normal distributions, which would be expected if the particles formed via agglomeration. This fact indicates that particle charging may be affecting the growth mechanism within the plasma.

Another surprising finding was that each plasma treatment changed the color of the material (Table 2). For example, titania treated in an argon plasma becomes black or dark gray. This suggests either a dramatic change in the absorption edge (unlikely), or a change in the surface composition of the particles.

Table 2 and Figure 12 clearly show carbon content of the surface correlates with color. The darkest samples contained the most surface carbon. The whitest samples contained much less surface carbon. The bulk composition analysis of the titania samples, both SEM and the dry combustion analysis, indicates that there is carbon present in P-25 and these techniques also show carbon content in the bulk is reduced by all plasma treatments. In particular, carbon was virtually eliminated by oxygen plasma treatment. The XPS results indicate that although argon plasma treatment reduced the bulk carbon, it did not reduce surface carbon. The carbon concentrations in the argon-treated sample and P-25 were virtually the same up to 150 Å sputtering depth. However, argon plasma treatments dramatically increased the carbon concentration at the immediate surface. In contrast, oxygen plasma treatment removes carbon from the titania. Finally, it should be noted that the blue coloration is not related to surface impurities, but rather to the oxygen stoichiometry in the surface layer. It is well known (Phillips 1981; Iyengar and Codell, 1972) that reduction in the oxygen concentration will shift the light absorption edge such that titania appears blue.

One last experimental note regards the impact of adding wetted argon (estimated to leave the bubbler in Figure 1 at >80% relative humidity) to the efficiency of spherodization. We hypothesized that adding water might allow direct absorption of field energy by wetted particles. Thus, not all energy would be transferred to the particles indirectly from hot electrons. The results were disappointing. The efficiency in all

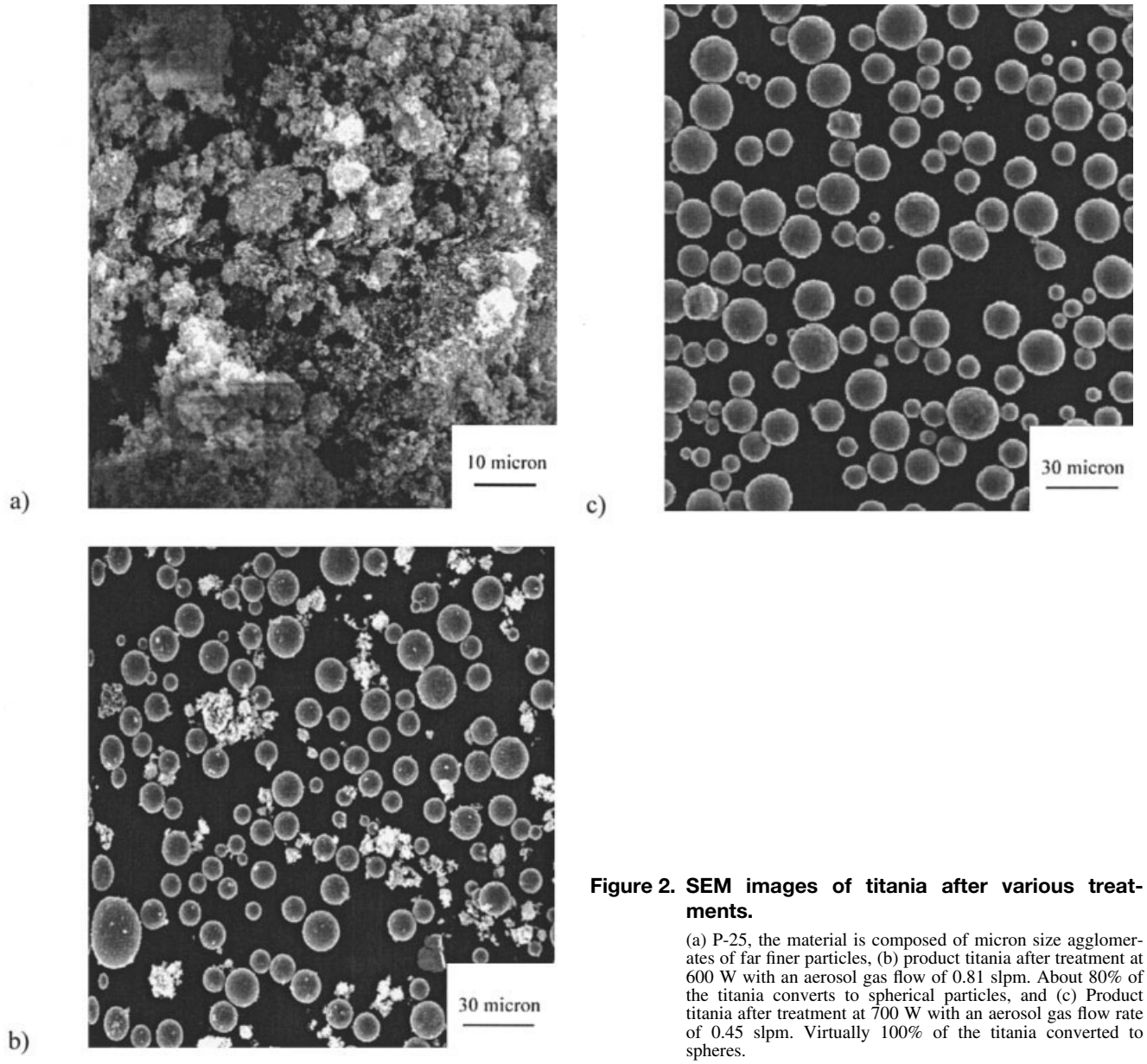

Figure 2. SEM images of titania after various treatments.

(a) P-25, the material is composed of micron size agglomerates of far finer particles, (b) product titania after treatment at 600 W with an aerosol gas flow of 0.81 slpm. About 80% of the titania converts to spherical particles, and (c) Product titania after treatment at 700 W with an aerosol gas flow rate of 0.45 slpm. Virtually 100% of the titania converted to spheres.

cases studied was slightly less than that observed with dry particles.

Discussion

We were able to show in this work that the process of titania spherodization is similar to that of alumina spherodization reported earlier. This supports our earlier contention that virtually any refractory oxide ceramic can be spherodized using the aerosol/plasma torch method. Indeed, in terms of the impact of operating parameters on surface area reduction, particle size, phase change, and efficiency of spherodization, there is a great similarity for these two ceramics. This suggests that the mechanism of titania spherodization is virtually identical to that of alumina spherodization. That is, particles melt in the hottest part of the plasma, agglomerate due to collisional processes, and then freeze into a spherical shape, primarily in the high-temperature phase, in the afterglow region.

There are several novel findings reported here. First, we demonstrated that particle charging, a process unique to plasma systems, may have some effect on the growth of the particles in the plasma. This finding is supported by a model which accounts for the effects of charging on particle collisions (next section). We also showed that single, spherodized particles often contained multiple phases. The process that leads to this unusual structure is due to rapid quenching of the molten particles after coming out of the torch. Finally, we showed that the plasma process could also lead to migration of impurities. In particular, we found that in both argon and oxygen plasmas carbon segregates to the surface. In the case of the oxygen plasma, this carbon is burned off, showing how an oxygen plasma can be used to purify ceramics.

Similarly to earlier work with alumina, the surface area (Figure 4) of plasma treated titania decreases simply because of loss of pore volume during melting and refreezing. The effect

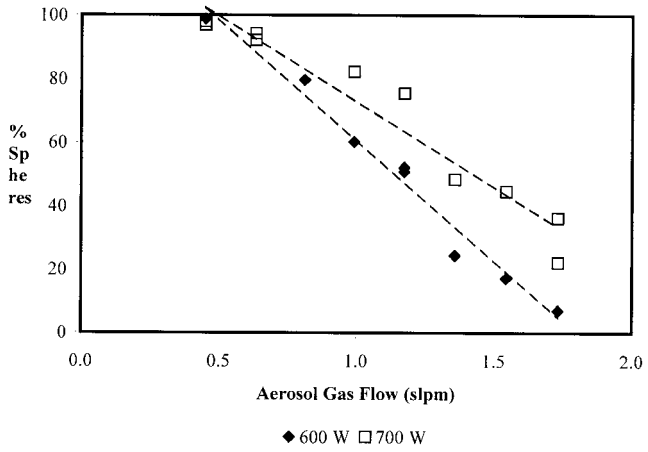

Figure 3. Effect of operating conditions on morphology.

Percentage spheres formed as a function of gas flow rate and absorbed power.

is enhanced as the flow rate is decreased because the increase of the residence time allows the particles to "condense" more. A second cause of surface area loss, again demonstrated in the work with alumina, is agglomeration and growth. The average diameter increases as the aerosol gas flow rate decreases because the particles have more residence time in the torch and hence have more collisions, leading to large particles. At higher power, we observed that the flame of the torch is longer than at lower power, which translates to longer residence times for the particles. Detailed spectroscopic analysis of an argon plasma in the same equipment supports the conclusion drawn from visual inspection (Chen, 2002), that the flame length increases with increasing power. With a longer flame (higher residience times) at higher power, more particle collisions occur and the product particles are larger.

The finding that the surface areas of the titania treated in oxygen plasma have more surface area than those treated in argon plasma may reflect the shorter residence times in oxygen plasmas compared to argon plasmas. That is, visual observation suggests the "hot zone" of oxygen plasmas is smaller than that

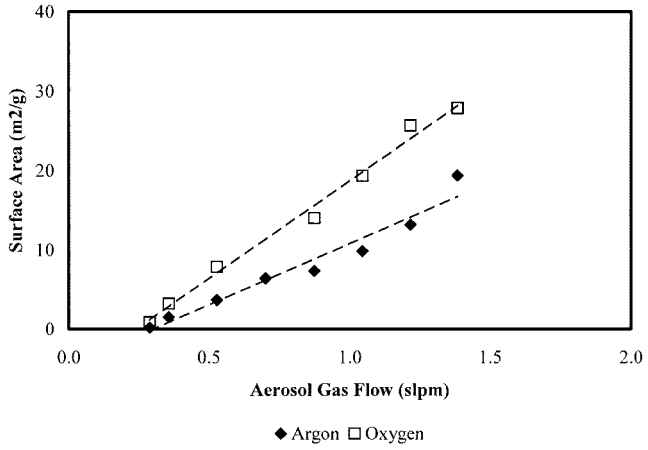

Figure 4. Effect of operating conditions on surface area.

Experiments conducted at 700W. The surface area of P-25 is 45 m^2/g.

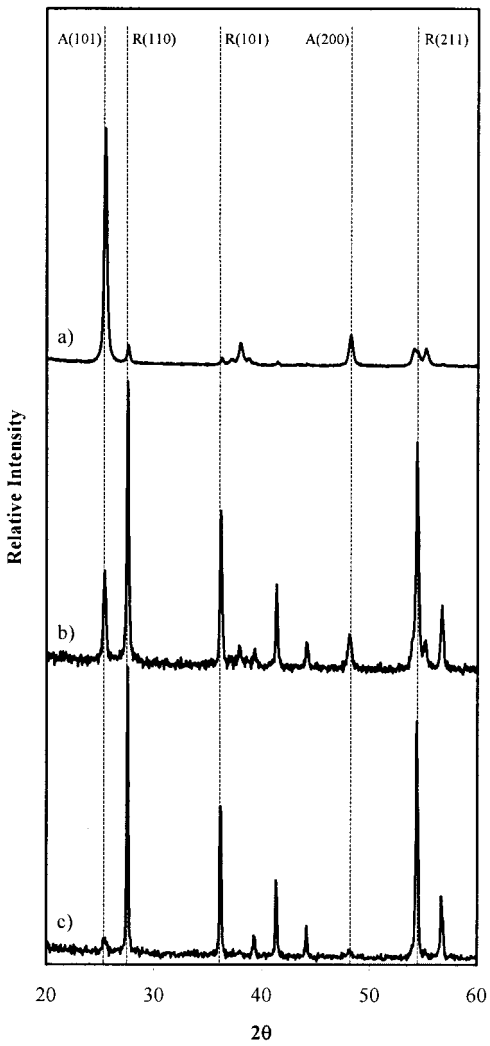

Figure 5. X-ray diffraction studies of untreated and treated titania.

(a) P-25, (b) Argon plasma treated titania at 80% spherodization, and (c) argon plasma treated titania at 95% spherodization. All experiments were at 700 W.

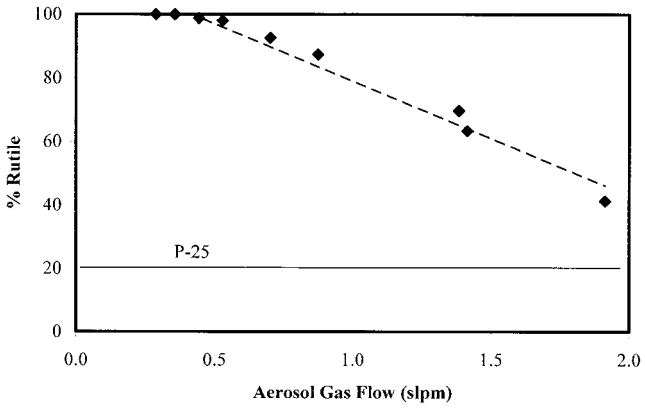

Figure 6. Variation of phase with gas flow rate.

Argon plasma, 700 W.

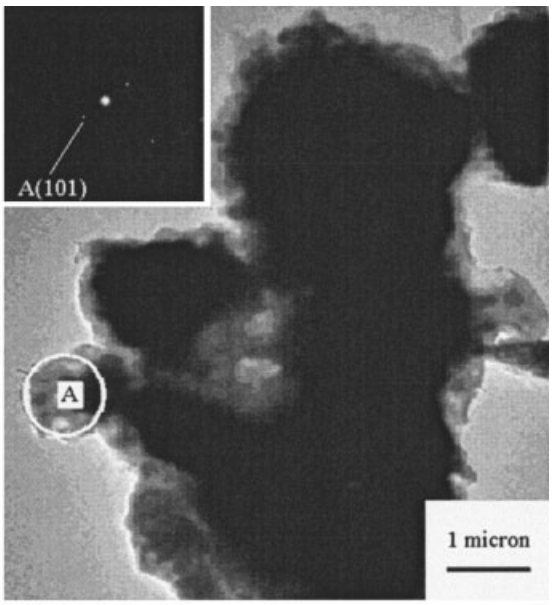

a)

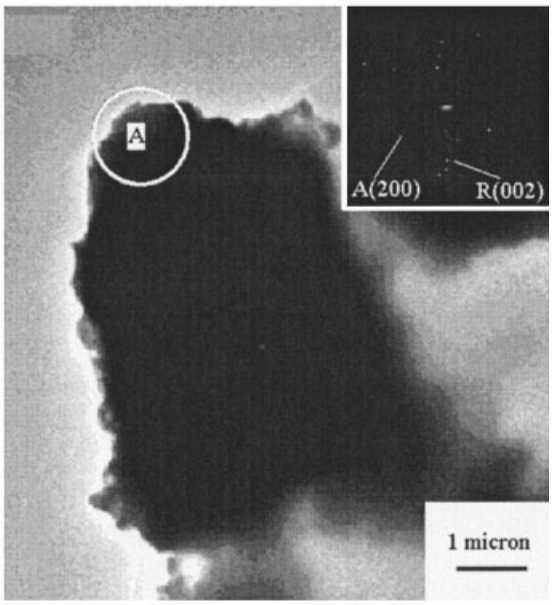

b)

Figure 7. Phase composition of individual titania particles by TEM-SAD.

(a) Particle containing only the rutile phase, and (b) particle containing both anatase and rutile phases. Argon plasma, 600 W, aerosol gas flow 1.2 slpm, 50% spherodization.

of argon plasmas operated under otherwise identical conditions.

The energy efficiency for spherodization (Figure 8) is proportional to the product of percentage spheres, and the mass flow rate. As long as the mass flow rate increases while maintaining 100% spherodization, the efficiency increases. It is clear that beyond a certain mass flow rate, further increases suddenly decrease the percentage of material converted to spheres, leading to an energy efficiency decrease. The decrease in the efficiency going from 0.53 slpm to 0.87 slpm is probably due to the fact that the energy transfer rate is not sufficient at the higher flow rate. A greater load can be processed at lower

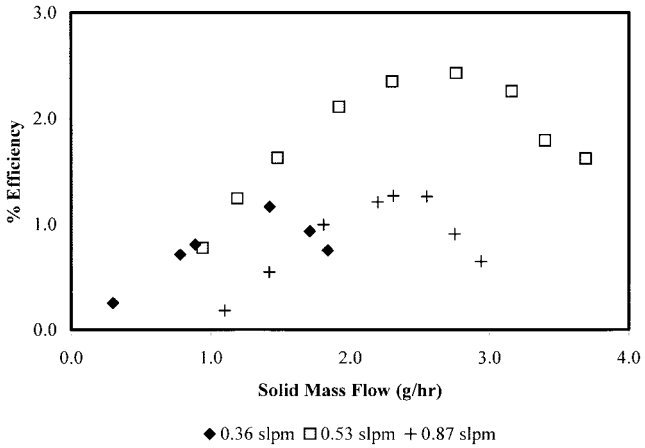

Figure 8. Energy efficiency for spherodization.

Argon plasma, 600 W.

flow rates as the particles reside in the plasma for a longer time. This conceptual model does not explain the low-maximum efficiency of the spheroidization observed at 0.36 slpm.

Treating the titania in the plasma torch altered the phases present in the material, similarly to what was seen with alumina. P-25 titania is a mixture of approximately 80% anatase and 20% rutile. As the solid passes through the torch and into the afterglow, its temperature first increases rapidly then decreases rapidly. This allows for the possibility of stabilizing a high-temperature phase. For titania, rutile is the thermodynamically favored phase at high-temperature, while anatase is favored at low-temperature. Because of the rapid quenching experienced by the particles, however, the majority of the treated titania is rutile. This process is analogous to quenching steel to stabilize high-temperature phases. One unique result of this work is that many of the titania spheres contain both phases.

There were also a number of phenomena observed with titania that were not observed in the alumina studies. Among the most significant is the purifying effect of an oxygen plasma. The titania treated in an argon plasma contained carbon on the

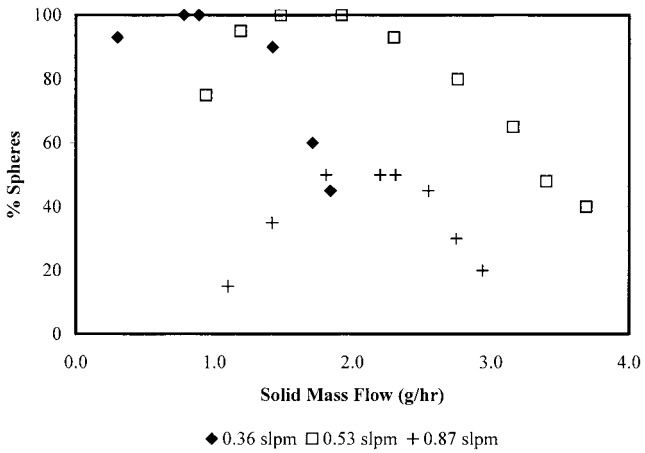

Figure 9. Effect of aerosol gas rate on the percentage of titania spherodized.

Argon plasma, 600 W.

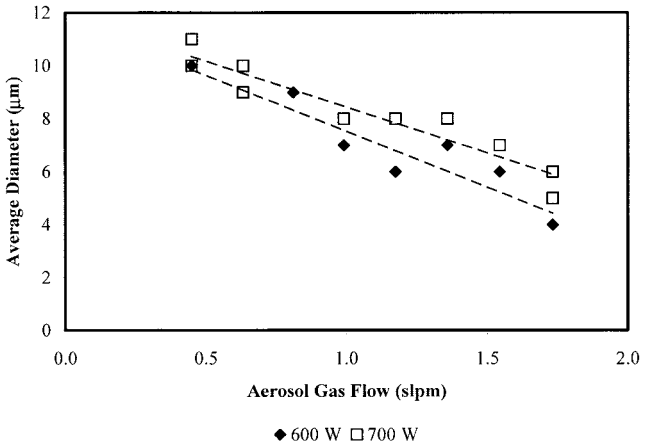

Figure 10. Dependence of particle size on aerosol gas flow rate.

Argon plasma.

surface, whereas the oxygen plasma treatment removed a portion of this carbon. We postulate that at the high-temperatures encountered in the plasma, a type of refining takes place, which drives carbon to the surface. In an oxygen plasma this carbon is combusted away, but it is left on the particle surfaces in an argon plasma.

Model Development

In order to begin understanding the impact of particle charging on agglomeration and growth, a model was developed to predict the behavior of the aerosol in the plasma. In microwave plasmas, the mobility of the electrons is much higher than that of the positive ions, leading to the accumulation of negative charge on all insulating surfaces, including titania particles in the aerosol. This leads to the generation of repulsive forces between particles. The experimental results demonstrate that growth via agglomeration took place, but raises the question of what effects, if any, repulsive forces created by particle charging had on particle growth.

The model used here is a simplified form of previous models developed to predict the effect of charging on particle growth (Kim, 2000; 2002; 2003). Kim et al. modeled the growth kinetics of "predator" and "protoparticles," incorporating the particle-charge distribution described by Matsoukas (Matsoukas and Russell, 1995; Matsoukas et al., 1996). In their model, they accounted for enhanced coagulation, due to the attraction between oppositely charged particles, and they assumed that particles of like charge never collide. Our model differs in two regards. First, we assume that all the particles of a given size possess the average charge given by Matsoukas (Lee and Matsoukas, 1999; Matsoukas and Russell, 1995). Second, our model looks specifically for conditions under which negatively charged particles do collide. That is, it elucidates the conditions under which the particles have sufficient kinetic energy to overcome the electrostatic repulsion. Our calculations are based on maximum electrostatic repulsion, for example screening is assumed to be negligible.

A two-charged-spheres model using an energy balance between potential (repulsion) and kinetic energy predicts a worst-case scenario for the impact of charging on growth by agglomeration. The model does not quantitatively predict particle growth; rather, it identifies the parameters having the greatest impact on particle growth. The elements of the model in brief: It is postulated that the two spheres are of equal size and carry the same amount of charge. The kinetic energy required to allow any two-charged particles to collide is estimated by integrating the repulsion force between them along the path from infinity to the collision point. Since the particles are carried as an aerosol, the velocity of each particle is estimated to equal some multiple (0.1, 1, or 5) of the velocity of the flow stream, and the relative velocity of the two particles at the collision point is also estimated to equal the particle velocity.

The above conditions provide an upper bound on the size of particles that will not collide due to surface charge induced repulsion. The particle velocity can indeed be higher than the gas velocity due to influences, such as ion drag, thermophoresis, and other factors (Choi and Kushner, 1994). Also, the effective repulsive force is probably screened at large distances by the ion sheath that forms around any negatively charged surface. There is also an argument that, at close distances, the repulsive force is reduced by particle/particle screening effects

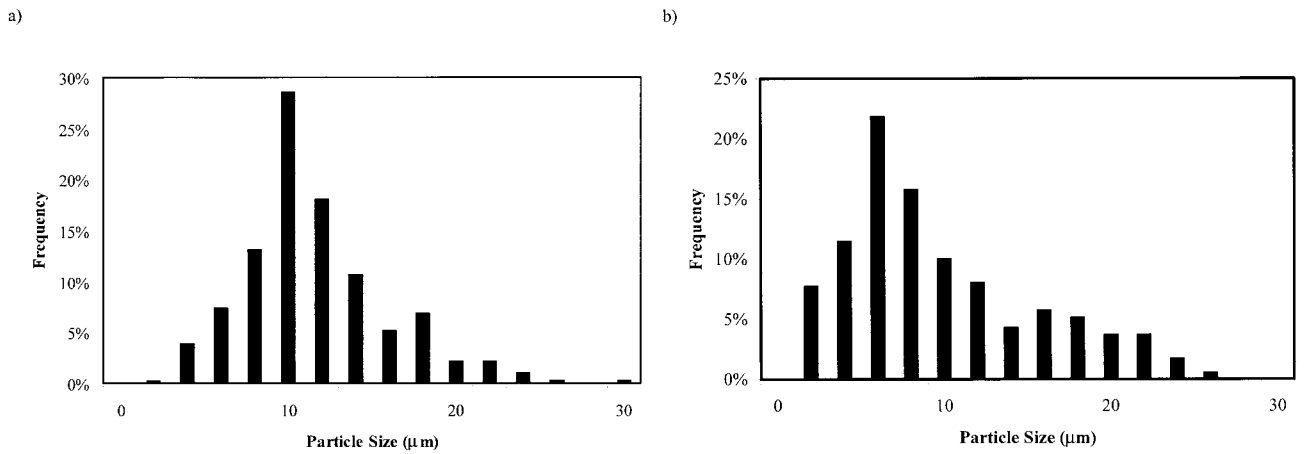

Figure 11. Particle-size distribution of spherodized titania.

Argon plasma, 700 W. (a) Aerosol gas flow of 0.45 slpm, (b) aerosol gas flow of 0.81 slpm. Distributions are based on at least 350 particles.

Table 2. Correlation of Color with Impurity Concentrations

		X-ray Emission (SEM)			Dry Combustion	XPS—Surface Analysis		
Sample	Color	%C	%Ti	%O	%C	%C	%Ti	%O
P-25	white	8.2	81.3	15.7	1.8 (1.2)	5.2	55.3	39.5
Argon Plasma	black	5.5	82.0	15.2	5.8	9.0	53.4	37.6
Oxygen Plasma	light blue	1.2	71.8	27.0	0.00 (0.01)	3.3	58.8	37.9

Bulk analysis was obtained using X-ray emission spectroscopy in SEM and dry combustion. Surface analysis was obtained via XPS. All compositions are weight percent, numbers in parenthesis represent duplicate analysis.

(Choi and Kushner, 1994). Also, but probably less likely, processes may be occurring in the plasma torch that allow nanosized particles (that is, primary particles) to collide. Recent studies (Matsoukas 1995; Lee and Masoukas, 1999) showed that particle charge fluctuated in the plasma. Such fluctuation could render these particles neutral or even perhaps positively charged for a brief moment to reduce the potential barrier created by electrostatic repulsive force. Thus, agglomeration process might still take places even if $E_{kinetic}/E_{repulsion}$ is less than one.

In this simple two-sphere model, if the kinetic energy is greater than the repulsion energy, and if the two particle centers are on the line of travel, the particles collide. The ratios of kinetic energy to repulsive energy ($E_{kinetic}/E_{repulsion}$) are plotted against various experimental operating conditions, as shown in Figure 13.

The diameter of the precursor agglomerates used in this study is about 3 μm. Thus, the model indicates that collision of agglomerates is not significantly impacted by charging effects under some conditions, but that it would be under others. Specifically, as shown in Figure 13c, the interparticle velocity is a critical factor in determining the role of particle charging. One conclusion from the model is that the agglomerates remain intact in the plasma, and that mechanical behavior is determined by agglomerate size and not primary particle size. The model predicts that nanoparticles would not agglomerate over any reasonable estimate of particle velocities. Thus, the absence of nanoparticles in the plasma-treated titania indicates that nanoparticles (primary particles) are not forming. In other words, evaporation (T_{vap}~2500–3000°C) and homogeneous nucleation of nanoparticles does not appear to be significant.

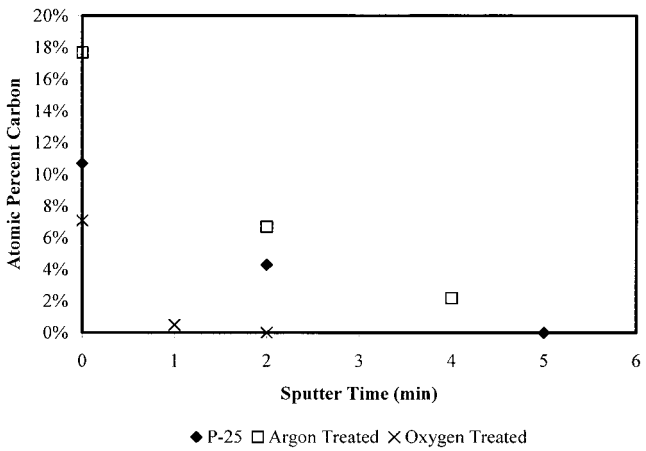

Figure 12. Carbon profile of treated and untreated titania.

Determined via XPS, 30 Å/min sputtering rate. All treated samples were prepared at 600 W.

This observation is reinforced by comparison with processes that lead to the generation of nanoparticles. Using the same apparatus, metal nanoparticles were made from a feedstock of micron sized metal particles (patent pending). In that case, the mechanism of nanoparticle generation requires complete evaporation of the precursor particles, followed by nucleation of new particles from the metal vapor. In this investigation, we find no evidence of nanoparticle formation, nor any other evidence of titania vaporization.

Nothing in our computations contradicts many earlier observations and calculations that indicate particle charging reduces the rate of agglomeration growth. Most of the earlier treatments focused on particles in the nanometer size range, where our model and earlier models agree charging can reduce the collision rate.

The model suggests that the particle-size distribution of plasma-produced particles may be significantly different than particles produced via ordinary agglomeration. As one example, collisions between two small particles are prohibited. This may explain why the observed particle-size distributions (see Figure 11) deviate from a log-normal distribution. Similar deviations were observed for restructuring alumina in the plasma torch (Shim et al., 1999).

The model results are the best that can be done with the existing data on the plasma, and they indicate areas that need further clarification. The model results suggest that the nature of particle agglomeration depends strongly on the plasma potential. It clearly identifies the need to map plasma potential, particle size, and particle velocity as a function of position. Such information could ultimately suggest operating and design strategies to maximize or minimize the volume of the plasma with high potential, according to the desired characteristics of the product particles.

Conclusions

The process of titania spherodization is similar to that of alumina spherodization reported earlier. The operating conditions dramatically impact the degree of spherodization, surface area, and phase of the products, the efficiency of spherodization, and the impurity concentration. The degree of spherodization increased with increasing power, and decreased with increasing aerosol gas flow. In all cases, the surface area decreased following plasma treatment. Individual titania spheres often contained multiple phases. The maximum energy efficiency for spherodization was 2.5%, as compared to 3.0% for alumina treatment. The dependence of the efficiency on operating parameters, such as the particle mass flow rate and

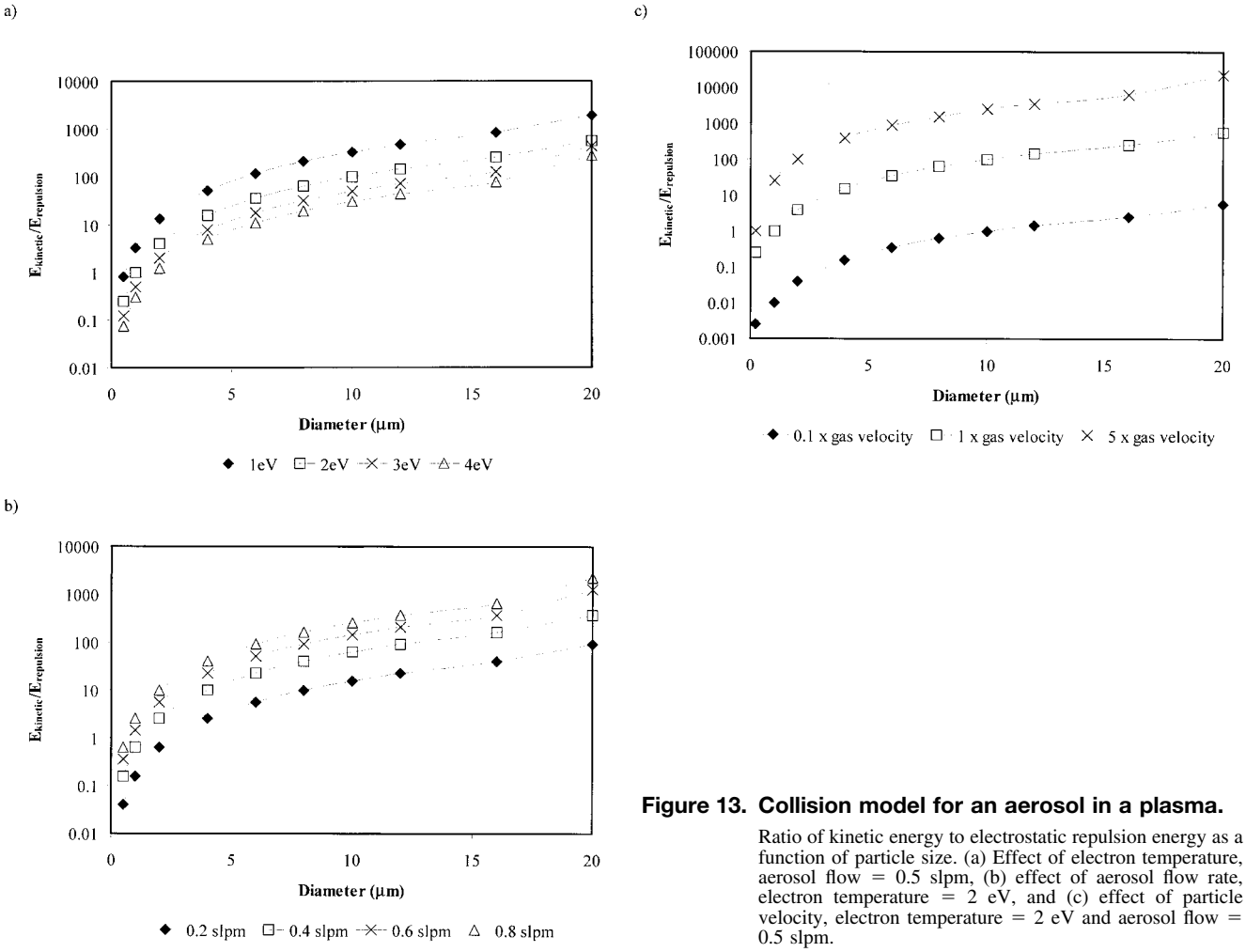

Figure 13. Collision model for an aerosol in a plasma.

Ratio of kinetic energy to electrostatic repulsion energy as a function of particle size. (a) Effect of electron temperature, aerosol flow = 0.5 slpm, (b) effect of aerosol flow rate, electron temperature = 2 eV, and (c) effect of particle velocity, electron temperature = 2 eV and aerosol flow = 0.5 slpm.

aerosol gas flow rate was complex. At a given aerosol gas flow rate, the efficiency increased until 100% spherodization could not be maintained, at which point it reached a maximum and then decreased. The dependence on aerosol gas flow was more complicated, and is not completely understood. The plasma process could also lead to migration and removal of impurities. Preliminary results indicate that these modified titanias are more active in photocatalytic oxidation of acetaldehyde than the precursor. Since so many physical properties change simultaneously during plasma treatment, the precise change that leads to improved photocatalytic activity is difficult to determine.

Literature Cited

Ameta, S. C., M. Bala, J. Kaur, and S. Sahasi, "Photocatalytic Reaction of Sodium-Nitroprusside," *Arabian J. Sci. Eng.* **19**, 71 (1994).

Ananthapadmanabhan, P. V., P. R. Taylor, and W. X. Zhu, "Synthesis of Titanium Nitride in a Thermal Plasma Reactor," *J. Alloys Compd.*, **287**, 126 (1999).

Bacsa, R. R., and J. Kiwi, "Effect of Rutile Phase on the Photocatalytic Properties of Nanocrystalline Titania During the Degradation of p-Coumaric Acid," *Appl. Catal. B: Environ.* **16**, 19 (1998).

Bennett, E. G., N. A. McKinnon, and L. S. Williams, "Sintering in Gas Discharges," *Nature (London)* **217**, 1287 (1968).

Brunauer, S., P. H. Emmet, and E. Teller, "Adsorption of Gases in Multimolecular Layers," *J. Am. Chem. Soc*. **60**, 309 (1938).

Carter, R. D., T. T. Broome, and S. C. Bacon, "Simultaneous Optimization of TiO2 Optical and Binder Demand in Coated Board Formulations Using Knowledge from the Paint Chemist," *Tappi J*. **81**, 185 (1998).

Chen, C.-K., T. C. Wei, L. R. Collins, and J. Phillips, "Modelling the Discharge Region of a Microwave Generated Hydrogen Plasma," *J. Phys. D: Appl. Phys.* **32**, 688 (1999).

Chen, C.-K., S. Gleiman, and J. Phillips, "Low-Power Plasma Torch Method for the Production of Crystalline Spherical Ceramic Particles," *J. Mater. Res.* **16**, 1256 (2001).

Chen, C.-K., and J. Phillips, "Impact of Aerosol Particles on the Structure of an Atmospheric Pressure Microwave Plasma Afterglow," *J. Phys. D: Appl. Phys*. **35**, 998 (2002).

Choi, S. J., and M. J. Kushner, "Mutual Shielding of Closely Spaced Dust Particles in Low-Pressure Plasmas," *J. Appl. Phys.,* **75**, 3351 (1994).

Cordone, L. G., and W. E. Martinsen, "Glow-Discharge Apparatus for Rapid Sintering of Al2O3," *J. Am. Ceram. Soc.,* **55**, 380 (1972).

Cullity, B. D., *Elements of X-ray Diffraction,* 2nd ed., Addison-Wesley Publishing Co. Reading, MA, pp. 415-417 (1978).

Diebold, M. P., "The Causes and Prevention of Titanium-Dioxide Induced Photodegradation of Paints.1. Theoretical Considerations and Durability," *Surf. Coat. Int*., **78**, 250 (1995).

Fauchais, P., A. Vardelle, and A. Denoirjean, "Reactive Thermal Plasmas: Ultrafine Particle Synthesis and Coating Deposition," *Surf. Coat. Technol.*, **97**, 66 (1997).

Fox, M. A., and M. T. Dulay, "Heterogeneous Photocatalysis," *Chem. Rev.,* Washington, DC, **93**, 341 (1993).

Gaumet, S., N. Siampiringue, J. Lemaire, and B. Pacaud, "Influence of Titanium Dioxide Pigment Characteristics on the Durability of Four Paints," *Surf. Coat. Int*., **80**, 367 (1997).

Gell, M., E. H. Jordan, Y. H. Sohn, D. Goberman, L. Shaw, and T. D. Xiao, "Development and Implementation of Plasma Sprayed Nanostructured Ceramic Coatings," *Surf. Coat. Technol.*, **146,** 48 (2001).
Hurum, D., A. G. Agrios, K. A. Gray, T. Rajh, and M. C. Thurnauer, "EPR Studies of Degussa P25 Photochemistry: Insight into Mixed Phase Titanium Dioxide Catalytic Activity," *Abstr. Pap.-Am. Chem. Soc*., **222**, U427 (2001).
Ishigaki, T., Y. Bando, Y. Moriyoshi, and M. Boulos, "Deposition from the Vapor-Phase During Induction Plasma Treatment of Alumina Powders," *J. Mater. Sci.,* **28**, 4223 (1993).
Iyengar, R. D., and M. Codell, "TiO2 and ZnO Surface Studies by Electron Spin Resonance Spectroscopy," *Adv. Colloid Interface Sci*., **3**, 365 (1972).
Johnson, D. L., and R. A. Rizzo, "Plasma Sintering of Beta-Alumina," *Ceram. Bull.*, **59**, 467 (1980).
Kim, K.-S., and D.-J. Kim, "Modeling of Rapid Particle Growth by Coagulation in Silane Plasma Reactor," *J. Appl. Phys.,* **87**, 2691 (2000).
Kim, D.-J., and K.-S. Kim, "Analysis on Nanoparticle Growth by Coagulation in Silane Plasma Reactor," *AIChE J.,* **48**, 2499 (2002).
Kim, K.-S., D.-J. Kim, J.-H. Yoon, J. Y. Park, Y. Watanabe, and M. Shiratani, "The Changes in Particle Charge Distribution During Rapid Growth of Particles in the Plasma Reactor," *J. Colloid Interface Sci,* **257**, 195 (2003).
Lee, K., and T. Matsoukas, "Can Charge Fluctuations Explain Particle Growth in Low-Pressure Plasmas?" *J. Appl. Phys.*, **85**, 2085 (1999).
Martin, S. T., J. M. Kesselman, W. Choi, and M. R. Hoffmann, "Surface-Structures and Photoreactivity : An FTIR-ATR Investigation of the Binding of Organic Substrates During the TiO2/UV Process," *Abstr. Pap.-Am. Chem. Soc.,* **210**, 223-ENVR (1995).
Matsoukas, T., and M. Russell, "Particle Charging in Low-Pressure Plasmas," *J. Appl. Phys.,* **77**, 4285 (1995).
Matsoukas, T., M. Russell, and M. Smith, "Stochastic Charge Fluctuations in Dusty Plasmas," *J. Vac. Sci. Technol. A*., **14**, 624 (1996).
Nelson, D. W., and L. E. Sommers, "Total Carbon, Organic Carbon, and Organic Matter," *Methods of Soil Analysis*, Vol. 2, 2nd ed., A. L. Page, R. H. Miller, and D. R. Keeney, eds., American Society of Agronomy, Madison, WI, 539 (1982).
Ohno, T., K. Sarukawa, K. Tokieda, and M. Matsumura, "Morphology of a TiO2 Photocatalyst (Degussa, P-25) Consisting of Anatase and Rutile Crystalline Phases," *J. Catal*., **203**, 82 (2001).
Phillips, J., "Morphological and Chemical Characterization of Catalysts Produced via the Thermal Decomposition of Iron Pentacarbonyl," Ph.D. Thesis, University of Wisconsin-Madison (1981).
Phillips, J., "Plasma Generation of Supported Metal Catalysts," *U.S. Patent* 5, **989**, 648 (1999).
Premkumar, J., and R. Ramaraj, "Photocatalytic Production of Hydrogen Peroxide Using Cellulose Adsorbed Titanium Dioxide Particles and Macrocyclic Cobalt(III) Complex," *Radiat. Phys. Chem.*, **49**, 115 (1997).
Rao, N. N., and S. Dube, "Photocatalytic Degradation of Mixed Surfactants and Some Commercial Soap Detergent Products Using Suspended TiO2 Catalysts," *J. Mol. Catal A: Chem*., **104**, L197 (1996).
Sadasivan, L. and U. R. Gandhi, "Colorant-Induced Exterior : Discoloration of Latex Paints," *J. Coat. Technol*.,**73**, 81 (2001).
Shim, H., J. Phillips, and I.S. Silva, "Restructuring of Alumina Particles Using a Plasma Torch," *J. Mater. Res*., **14**, 849 (1999).
Thomas, G., and J. Freim, "Parametric Investigation of the Glow Discharge Technique for Sintering UO2," *Trans. Am. Nucl. Soc*., **21**, 65 (1975).
Wicks, Z. W., F. N. Jones, and S. P. Pappas, "Pigment Dispersion: III," *J. Coat. Technol*., **73**, 77 (2001).
Williams, D. B., and C. B. Carter, *Transmission Electron Microscopy: A Textbook for Materials Science,* Plenum Press, New York, NY (1996).
Ziolli, R. L., and W. F. Jardim, "Mechanism Reactions of Photodegradation of Organic Compounds Catalyzed by TiO2," *Quim. Nova.,* **21**, 319 (1998).

Manuscript received Feb. 13, 2003, and revision received Dec. 16, 2003.